ACS APPLIED MATERIALS & INTERFACES

Research Article

www.acsami.org

High-Performance NiO/Ag/NiO Transparent Electrodes for Flexible Organic Photovoltaic Cells

Zhichao Xue,[‡,†] Xingyuan Liu,*[,†] Nan Zhang,[†] Hong Chen,[§] Xuanming Zheng,[§] Haiyu Wang,[∥] and Xiaoyang Guo*[,†]

[†]State Key Laboratory of Luminescence and Applications, Changchun Institute of Optics, Fine Mechanics and Physics, Chinese Academy of Sciences, Changchun 130033, China

[‡]University of Chinese Academy of Sciences, Beijing 100049, China

[§]Key Laboratory of Optical System Advanced Manufacturing Technology, Chinese Academy of Sciences, Changchun 130033, China

[∥]State Key Laboratory on Integrated Optoelectronics, College of Electronic Science & Engineering, Jilin University, Changchun, 130012, China

Supporting Information

ABSTRACT: Transparent electrodes with a dielectric−metal−dielectric (DMD) structure can be implemented in a simple manufacturing process and have good optical and electrical properties. In this study, nickel oxide (NiO) is introduced into the DMD structure as a more appropriate dielectric material that has a high conduction band for electron blocking and a low valence band for efficient hole transport. The indium-free NiO/Ag/NiO (NAN) transparent electrode exhibits an adjustable high transmittance of ∼82% combined with a low sheet resistance of ∼7.6 $\Omega \cdot s \cdot q^{-1}$ and a work function of 5.3 eV after UVO treatment. The NAN electrode shows excellent surface morphology and good thermal, humidity, and environmental stabilities. Only a small change in sheet resistance can be found after NAN electrode is preserved in air for 1 year. The power conversion efficiencies of organic photovoltaic cells with NAN electrodes deposited on glass and polyethylene terephthalate (PET) substrates are 6.07 and 5.55%, respectively, which are competitive with those of indium tin oxide (ITO)-based devices. Good photoelectric properties, the low-cost material, and the room-temperature deposition process imply that NAN electrode is a striking candidate for low-cost and flexible transparent electrode for efficient flexible optoelectronic devices.

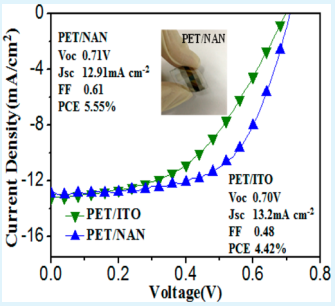

KEYWORDS: *flexible electronics, NiO, organic photovoltaic cells, transparent electrode*

INTRODUCTION

Organic photovoltaic (OPV) cells have unique properties including low weight, flexibility, low cost, and suitability for large-scale production, making them very attractive as a renewable energy source. In particular, flexible OPV cells have potentials to assemble on clothing, tents, flexible chargers, and packaging that can be folded into smaller volumes for convenient carrying.[1] Although their power conversion efficiency (PCE) has reached over 9% with recent rapid progress in OPV technology and interfacial materials,[2,3] OPV devices with flexible substrates have improved more slowly because of the scarcity of flexible transparent electrodes with excellent optoelectrical properties. Indium tin oxide (ITO) is the most commonly used material for transparent electrodes,[4] but its brittleness and high-temperature processing limit its utility for flexible devices.[5] Furthermore, the growing cost of indium has led to increasing costs of devices based on ITO electrodes.

Several alternatives to ITO have been reported, such as carbon nanotubes,[6−9] conducting polymers,[10−12] graphene,[13−16] metallic film,[17] metallic nanowires,[18−20] and metallic grids.[21−23] However, many of these alternative materials suffer from either large sheet resistance[9,14] or high surface roughness,[18−21] which cause reduced fill factors (FF) and PCEs for OPV devices. Therefore, novel transparent electrodes with good optoelectrical properties and mechanical flexibility, together with low costs and low-temperature processing, still remain a big challenge.

Recently, dielectric−metal−dielectric (DMD) electrodes have aroused great concerns as transparent electrodes with good optical and electrical properties in a simple fabrication process.[24−27] The electrical properties of DMD electrodes mainly depend on the metal layer, and the transmittance of DMD electrodes can be enhanced by introducing two dielectric layers with high refractive indexes at both sides of the metal layer.[28−30] In addition, the work function of DMD electrodes can be managed through the choice of the dielectric, which can allow them to be used as cathodes, anodes, or intermediate electrodes in tandem solar cells. Hole transport materials such as WO_3[26,31] and MoO_3[32,33] and electron transport materials such as TiO_2[34] and ZnO[35] have been introduced in the DMD structure for transparent anode and cathode, respectively. And

Received: July 23, 2014
Accepted: August 22, 2014
Published: August 22, 2014

flexible OPVs based on DMD electrodes have exhibited properties competitive with those of rigid devices based on ITO electrodes.[24] However, the stability of DMD electrodes are seldom reported, which is a key performance from a practical standpoint. Another drawback could be that most dielectrics used in high-work-function DMD anodes do not have an ideal conduction band for the suppression of undesirable carrier recombination at the interface.

Recently, nickel oxide (NiO) was introduced as an anode interfacial layer in OPVs with a high conduction band energy for electron blocking but a suitable valence band for effective hole transport.[36,37] Such properties make it a more appropriate dielectric candidate for DMD structure. In this study, a NiO dielectric layer is employed to construct a DMD electrode for the first time for flexible OPVs. A transparent electrode with a NiO/Ag/NiO (NAN) structure deposited on a polyethylene terephthalate (PET) substrate shows excellent electrical, optical, and mechanical properties, together with good thermal, moisture, and environmental stability, making its performance comparable to or better than those of ITO electrodes. This indicates that the flexible transparent NAN electrode is a striking candidate for replacing ITO in efficient optoelectronic devices.

RESULTS AND DISCUSSION

The properties of DMD structures depend on the thickness of each layer. The threshold thickness value of the metal layer is usually around 10 nm, above which the multilayer structures change from an insulating state to a highly conductive state. This change is attributed to the percolation of conducting metal paths. The transmittance of the films increases when the metal thickness increases up to the percolation threshold, while further increases reduce the transmittance.[38] Therefore, an 11 nm thick Ag layer was introduced to ensure a low sheet resistance, while the thicknesses of two NiO layers were varied to optimize the optical transmittance of the NAN electrodes. Figure 1a shows the calculated average transmittance values of NAN electrodes with different NiO thicknesses over the wavelength range from 400 to 800 nm. It can be seen that the transmittance of the NAN electrode can be precisely modulated by controlling the thickness of the NiO layer. As the NiO thickness increases, the average transmittance of the NAN electrode climbs and then declines after a maximum value of 80% for two 35 nm thick NiO layers. The measured transmittance spectra of NAN electrodes with different NiO thickness are consistent with the calculated spectra (Supporting Information, Figure S1). Thus, the NAN electrode with the optimized NiO (35 nm)/Ag (11 nm)/NiO (35 nm) structure was employed as a transparent electrode for an OPV and was found to allow efficient light absorption in the photoactive layer. Figure 1b shows the transmittance spectra of NAN and ITO electrodes on glass and PET substrates, respectively. The NAN electrode on the glass substrate exhibits a maximum transmittance of 82% and an average transmittance of 79% over the visible range (400−700 nm), whereas the NAN electrode on the PET substrate exhibits a maximum transmittance of 80% and an average transmittance of 77% over the same range. For comparison, the average transmittances of glass/ITO and PET/ITO structures were also measured over the visible range and were found to be 85 and 82%, respectively.

To study the electrical properties, we carried out a Hall measurement. A NAN multilayer with a NiO (35 nm)/Ag (11 nm)/NiO (35 nm) structure shows *n*-type properties, and its

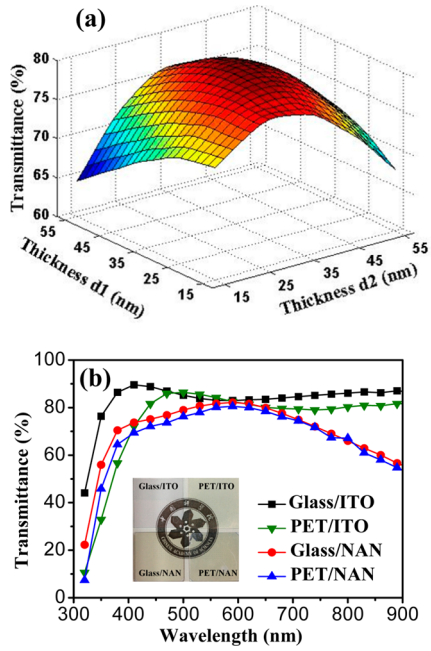

Figure 1. (a) Calculated average transmittance of glass/NAN structures in the wavelength range from 400 to 800 nm as a function of the thickness of the two NiO layers. The thickness of Ag is fixed at 11 nm. (b) Measured transmittance spectra of ITO and NAN films on glass and PET substrates.

carrier concentration, resistivity, and carrier mobility are 7.371 × 10^{21} cm^{-3}, 6.169 × 10^{-5} Ω·cm, and 13.73 $cm^2 \cdot V^{-1} \cdot s^{-1}$, respectively. Thus, a calculated sheet resistance of 7.6 $\Omega \cdot s \cdot q^{-1}$ was achieved, which is lower than that of most commercial ITO electrodes.[39]

The surface roughness and work function of transparent electrodes are very important properties that affect the stability and efficiency of OPVs.[40−42] The NAN electrode based on the PET substrate also shows an excellent surface morphology for use as a transparent electrode for flexible and efficient OPVs. Figure 2 shows atomic force microscopy (AFM) images of the ITO and NAN electrodes. The ITO electrode has a squama-like morphology with a root-mean-square (RMS) roughness of 2.52 nm, whereas the NAN deposited on PET has small exposed grain-like features and an RMS of only 1.73 nm. The work function of NiO can be tuned between 4.5 and 5.6 eV by using different processing conditions.[36,43] Here, the work

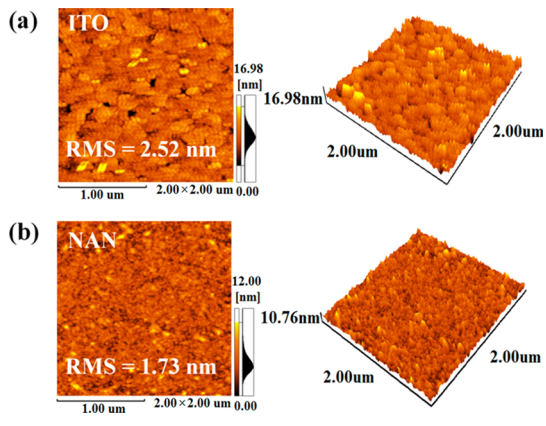

Figure 2. AFM images of (a) ITO and (b) NAN.

dx.doi.org/10.1021/am504806k | ACS Appl. Mater. Interfaces 2014, 6, 16403−16408

function of the NAN electrode was measured by a Kelvin probe system to be 4.7 eV without any treatment. However, the work function of the NAN electrode can be increased by ultraviolet ozone (UVO) treatment (Supporting Information, Figure S2). After 10 min of UVO treatment, the work function of NAN electrode increased to 5.3 eV because of the formation of NiOOH species, which results in a large surface dipole and an increased work function.[36,43] The decreased offset between the work function of the NAN electrode and the highest occupied molecular orbital level of the donor polymer (Supporting Information, Figure S3) indicates good ohmic contact, and the resulting increased built-in potential for maximizing the open-circuit voltage (V_{OC}) will allow NAN devices to be operated without any interfacial layers at the anode.

The stability of flexible electrodes to mechanical stress, temperature, humidity, and environmental conditions has significant effects on the performance of flexible devices. Figure 3a–c shows the electrical characteristics, including the carrier

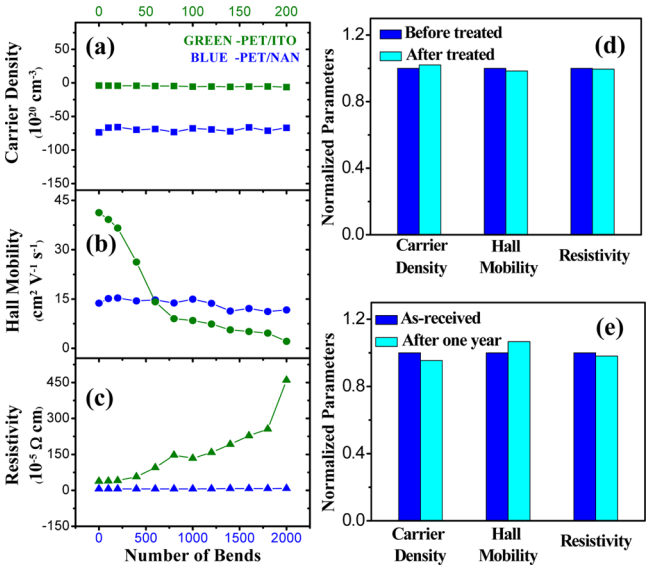

Figure 3. (a) Carrier density, (b) Hall mobility, and (c) resistivity of the PET/ITO and PET/NAN flexible electrodes after repeated bending. The green curves are for the PET/ITO (top x axis) electrode, and the blue curves are for the PET/NAN (bottom x axis) electrode. The bending angle was about 90°. (d) Carrier density, Hall mobility, and resistivity before and after the NAN electrode was stored at a constant temperature of 60 °C and relative humidity of 90% for 24 h. (e) Normalized changes in carrier density, Hall mobility, and resistivity of the NAN electrode before and after it was preserved in air for 1 year.

concentration, Hall mobility, and resistivity of the NAN and ITO flexible electrodes under repeated bending. The bending angle was about 90° (Supporting Information, Figure S6). Even after 2000 bending cycles, the carrier concentration and Hall mobility of the NAN electrode remain virtually unchanged, and the sheet resistance increases only slightly from 7.6 to 9.8 $\Omega \cdot s \cdot q^{-1}$. In contrast, because of the brittleness of ITO, the sheet resistance of the flexible ITO increases dramatically from 38 to about 414.4 $\Omega \cdot s \cdot q^{-1}$ after only 200 bending cycles. In addition, the Hall mobility of the flexible ITO electrode decreases from 41.29 to 2.15 $cm^2 \cdot V^{-1} \cdot s^{-1}$. These results illustrate that our flexible NAN electrodes have better mechanical properties than flexible ITO electrodes.

The stability of the NAN electrode to temperature and humidity was investigated by putting the NAN electrode in a controlled environment with a constant temperature of 60 °C and relative humidity of 90% for 24 h. Figure 3d shows the electrical properties of the NAN electrode before and after this heat and humidity treatment. It is found that the NAN electrode was very stable, especially in terms of its sheet resistance, which remained 7.6 $\Omega \cdot s \cdot q^{-1}$ after this treatment. For comparison, a 10 nm Ag layer was put in the same environment, and the resistivity of the Ag electrode increased by 30% (Supporting Information, Figure S7), which illustrates the NiO layer effectively protects the Ag layer. More importantly, after the NAN electrode was preserved in air for 1 year, it showed only a small change of about 1.8% in sheet resistance (Figure 3e). Therefore, the NAN electrode exhibits excellent flexibility together with good thermal, moisture, and environmental stability and is suitable for use in stable and efficient OPVs.

To evaluate the properties of the transparent NAN electrode, we prepared OPVs based on a conjugated polymer consisting of poly[4,8-bis(2-ethylhexyloxy)-benzo[1,2-*b*:4,5-*b*′] dithiophene-2,6-diyl-*alt*-4-(2-ethylhexyloxy)-thieno[3,4-*b*]thiophene-2,6-diyl] (PBDTTT-C) and [6,6]-phenyl C71-butyric acid methyl ester ($PC_{70}BM$) on NAN electrodes on glass and PET substrates. Figure 4 shows the structures and properties of the

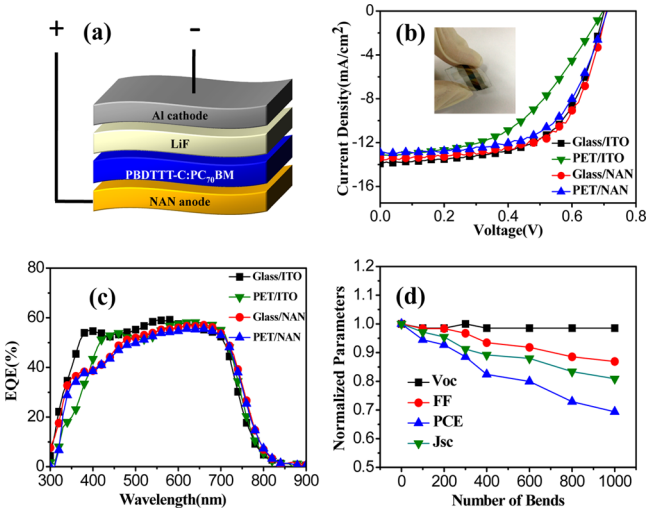

Figure 4. (a) Configuration of the OPV based on the NAN electrode. (b) J–V characteristics and (c) EQE spectra of the OPVs based on ITO and NAN electrodes on glass and PET substrates. (d) Normalized cell parameters of the flexible OPV as a function of the number of bending cycles. The bending angle was about 90°.

OPV devices, and the energy level alignment of the OPV devices is shown in Figure S3 (Supporting Information). For comparison, similar devices using traditional ITO/poly(3,4-ethylene dioxythiophene)-polystyrene sulfonic acid (PEDOT:PSS) electrodes were also fabricated. Figure 4b shows the J–V characteristics of the OPVs under 100 $mW \cdot cm^{-2}$ AM 1.5 G illumination. Detailed performance parameters of the OPVs are listed in Table 1. For the device with glass/ITO as the anode, a PEDOT/PSS buffer layer was employed for hole transport, and a PCE of 5.90% was obtained with a short-circuit current density (J_{SC}) of 13.92 $mA \cdot cm^{-2}$, a V_{OC} of 0.70 V, and a FF of 0.61. The glass/NAN device showed a slightly lower J_{SC} of 13.37 $mA \cdot cm^{-2}$, a V_{OC} of 0.71 V, and a higher FF of 0.64,

dx.doi.org/10.1021/am504806k | ACS Appl. Mater. Interfaces 2014, 6, 16403–16408

Table 1. Performance of OPVs based on Different Substrates

device	V_{oc} (V)	J_{sc} (mA cm^{-2})	FF	PCE (%)	Rs (Ω cm^2)
glass/ITO/PEDOT	0.70 ± 0.02	13.92 ± 0.20	0.61 ± 0.01	5.90 ± 0.20	5.2
glass/NAN	0.71 ± 0.01	13.37 ± 0.25	0.64 ± 0.01	6.07 ± 0.18	4.6
PET/ITO/PEDOT	0.70 ± 0.01	13.20 ± 0.25	0.48 ± 0.01	4.42 ± 0.25	18.2
PET/NAN	0.71 ± 0.01	12.91 ± 0.20	0.61 ± 0.01	5.55 ± 0.15	6.4

resulting in a higher PCE of 6.07%. When a flexible PET/ITO structure was used as the anode, a PCE of 4.42% was achieved with a J_{SC} of 13.20 mA·cm^{-2}, a V_{OC} of 0.70 V, and a FF of 0.48. Finally, the device with the PET/NAN electrode showed a higher PCE of 5.55% with a J_{SC} of 12.91 mA·cm^{-2}, a V_{OC} of 0.71 V, and a FF of 0.61. The series resistances (R_s) of the four devices calculated from the $J-V$ curves under light are also shown in Table 1. Compared with the ITO devices, which had R_s values of 5.2 Ω cm^2 for the glass substrate and 18.2 Ω·cm^2 for the PET substrate, the devices based on NAN anodes showed lower R_s values of 4.6 Ω·cm^2 for the glass substrate and 6.4 Ω·cm^2 for the PET substrate, resulting in higher FFs and PCEs. A higher R_s of PET/ITO can be assumed to be the deterioration of conductivity of ITO due to the inevitable substrate vibration in the process of OPV fabrication. Because of the lower transmittance of the NAN electrode, the NAN devices show smaller J_{SC} values, which limits the light absorption in the active layer. This result was confirmed by the external quantum efficiency (EQE) spectra of the devices based on different substrates (Figure 4c). Figure 4d shows the results obtained for the flexible OPV under repeated bending. As can be seen, for the photovoltaic device with the NAN electrode, as the number of bends increases, both the J_{SC} and FF decay gradually (19.1% and 13.1% decreases in J_{SC} and FF, respectively, after 1000 bending cycles), while V_{OC} remains constant. However, 69.4% of its initial PCE was retained after 1000 bending cycles. The evolutions of photovoltaic parameters of NAN and ITO based OPVs under bending at different angles were also studied (Supporting Information, Figure S8), which illustrates that NAN-based OPVs have better flexibility than ITO-based devices.

CONCLUSION

In conclusion, we have developed an indium-free transparent electrode with a NiO/Ag/NiO structure. The NAN electrode shows excellent optical and electrical properties, including an adjustable high transmittance of 82% and a low sheet resistance of ~7.6 Ω·s·q^{-1}. The PCEs of OPVs with NAN electrodes deposited on glass and PET substrates are 6.07 and 5.55%, respectively, which are competitive with those of ITO-based devices. Both the flexible NAN electrode itself and OPVs fabricated with these electrodes show excellent stability to bending-induced tension stress, and the NAN electrode also exhibits good stability to temperature, humidity, and environmental conditions. Mass production of NAN on flexible substrate by roll-to-roll magnetron sputtering technologies can be realized. The low-cost material and the room-temperature deposition process means that NAN transparent electrodes not only have good photoelectric properties, but also have a very high ratio of performance to price in efficient flexible OPVs.

EXPERIMENTAL METHODS

NAN Electrode Fabrication and Characterization. The NAN films were deposited on a precleaned polished glass substrate by electron beam evaporation at room temperature. The thickness of the NiO layers was varied between 15 and 55 nm, whereas the silver layer thickness was fixed at 11 nm. The evaporation rates of NiO and Ag were 0.09−0.12 and 0.7−1.0 nm/s, respectively, at pressures below 2.0 × 10^{-3} Pa. The sheet resistance was measured using a four-probe method. The carrier concentration and Hall mobility of the NAN films were determined using an HMS-3000 Hall effect measurement system with an applied magnetic field of 0.55 T. The surface work function of the NAN films was measured using a KP Technology Ambient Kelvin probe system package. The film thicknesses were calibrated with an Ambios XP-1 surface profiler. The transmittance spectra of the NAN samples were recorded using a Shimadzu UV-3101PC spectrophotometer. The AFM measurement was performed on a Shimadzu SPM-9700. The temperature and humidity stabilities of the NAN electrode were measured using a SUYING test instrument. All measurements of the optoelectrical properties were performed at room temperature.

OPV Fabrication and Characterization. NiO (35 nm), Ag (11 nm), and NiO (35 nm) were deposited sequentially by electron beam evaporation through a shadow mask under room tempreture. After 10 min of UVO treatment, an active layer consisting of a blend of the low-bandgap conjugated polymer PBDTTT-C (Solarmer) and $PC_{70}BM$ (American Dye) was spin-coated onto the substrates from dichlorobenzene in a glovebox. A small amount (3% in volume ratio) of a high-boiling-point additive, 1,8-diiodooctane (DIO, Sigma-Aldrich), was used in order to optimize the morphology. Finally, LiF (1 nm) and Al (100 nm) were thermally deposited at a pressure of approximately 4 × 10^{-4} Pa. The $J-V$ characteristics of the OPVs were measured using a computer-controlled Keithley 2611 source meter under AM 1.5 G illumination from a calibrated Solar with an irradiation intensity of 100 mW·cm^{-2}. EQE measurements were performed with a lock-in amplifier at a chopping frequency of 20 Hz under illumination by monochromatic light from a xenon lamp.

ASSOCIATED CONTENT

Supporting Information

Simulated transmittance, work function, energy level, electric field distribution, and SEM. This material is available free of charge via the Internet at http://pubs.acs.org.

AUTHOR INFORMATION

Corresponding Authors

*E-mail: liuxy@ciomp.ac.cn.
*E-mail: guoxy@ciomp.ac.cn.

Notes

The authors declare no competing financial interest.

ACKNOWLEDGMENTS

This work is supported by the CAS Innovation Program, National Science Foundation of China (Nos. 51102228, 61106057), the Jilin Province Science and Technology Research Project (No. 20140520119JH), and the State Key Laboratory of Luminescence and Applications.

REFERENCES

(1) Morton, O. Solar Energy: Silicon Valley Sunrise. *Nature* **2006**, *443*, 19−22.

(2) He, Z.; Zhong, C.; Su, S.; Xu, M.; Wu, H.; Cao, Y. Enhanced Power-Conversion Efficiency in Polymer Solar Cells Using an Inverted Device Structure. *Nat. Photonics* **2012**, *6*, 591−595.
(3) Li, W.; Furlan, A.; Hendriks, K. H.; Wienk, M. M.; Janssen, R. A. J. Efficient Tandem and Triple-Junction Polymer Solar Cells. *J. Am. Chem. Soc.* **2013**, *135*, 5529−5532.
(4) Choi, J. K.; Jin, M. L.; An, C. J.; Kim, D. W.; Jung, H. T. High-Performance of PEDOT/PSS Free Organic Solar Cells on an Air-Plasma-Treated ITO Substrate. *ACS Appl. Mater. Interfaces* **2014**, *6* (14), 11047−11053.
(5) Hecht, D. S.; Hu, L.; Irvin, G. Emerging Transparent Electrodes Based on Thin Films of Carbon Nanotubes, Graphene, and Metallic Nanostructures. *Adv. Mater.* **2011**, *23*, 1482−1513.
(6) Wu, Z.; Chen, Z.; Du, X.; Logan, J. M.; Sippel, J.; Nikolou, M.; Kamaras, K.; Reynolds, J. R.; Tanner, D. B.; Hebard, A. F.; Rinzler, A. G. Transparent, Conductive Carbon Nanotube Films. *Science* **2004**, *305*, 1273−1276.
(7) Tenent, R. C.; Barnes, T. M.; Bergeson, J. D.; Ferguson, A. J.; To, B.; Gedvilas, L. M.; Heben, M. J.; Blackburn, J. L. Ultrasmooth, Large-Area, High-Uniformity, Conductive Transparent Single-Walled-Carbon-Nanotube Films for Photovoltaics Produced by Ultrasonic Spraying. *Adv. Mater.* **2009**, *21*, 3210−3216.
(8) Barnes, T. M.; Reese, M. O.; Bergeson, J. D.; Larsen, B. A.; Blackburn, J. L.; Beard, M. C.; Bult, J.; Lagemaat, J. Comparing the Fundamental Physics and Device Performance of Transparent, Conductive Nanostructured Networks with Conventional Transparent Conducting Oxides. *Adv. Energy Mater.* **2012**, *2*, 353−360.
(9) Salvatierra, R. V.; Cava, C. E.; Roman, L. S.; Zarbin, A. J. G. ITO-Free and Flexible Organic Photovoltaic Device Based on High Transparent and Conductive Polyaniline/Carbon Nanotube Thin Films. *Adv. Funct. Mater.* **2013**, *23*, 1490−1499.
(10) Ha, Y. H.; Nikolov, N.; Pollack, S. K.; Mastrangelo, J.; Martin, B. D.; Shashidhar, R. Towards a Transparent, Highly Conductive Poly(3,4-ethylenedioxythiophene). *Adv. Funct. Mater.* **2004**, *14*, 615−622.
(11) Kirchmeyer, S.; Reuter, K. Scientific Importance, Properties and Growing Applications of Poly(3,4-ethylenedioxythiophene). *J. Mater. Chem.* **2005**, *15*, 2077−2088.
(12) Vosgueritchian, M.; Lipomi, D. J.; Bao, Z. Highly Conductive and Transparent PEDOT:PSS Films with a Fluorosurfactant for Stretchable and Flexible Transparent Electrodes. *Adv. Funct. Mater.* **2012**, *22*, 421−428.
(13) Wu, J. B.; Agrawal, M.; Becerril, H. A.; Bao, Z. N.; Liu, Z. F.; Chen, Y. S.; Peumans, P. Organic Light-Emitting Diodes on Solution-Processed Graphene Transparent Electrodes. *ACS Nano* **2010**, *4*, 43−48.
(14) De, S.; Coleman, J. N. Are There Fundamental Limitations on the Sheet Resistance and Transmittance of Thin Graphene Films? *ACS Nano* **2010**, *4*, 2713−2720.
(15) Yin, Z.; Sun, S.; Salim, T.; Wu, S.; Huang, X.; He, Q.; Lam, Y. M. Organic Photovoltaic Devices Using Highly Flexible Reduced Graphene Oxide Films as Transparent Electrodes. *ACS Nano* **2010**, *4*, 5263−5268.
(16) Chen, X.; Jia, B.; Zhang, Y.; Gu, M. Exceeding the Limit of Plasmonic Light Trapping in Textured Screen-Printed Solar Cells Using Al Nanoparticles and Wrinkle-like Graphene Sheets. *Light: Sci. Appl.* **2013**, *2*, e92.
(17) Su, H.; Zhang, M.; Chang, Y. H.; Zhai, P.; Hau, N. Y.; Huang, Y. T.; Liu, C.; Soh, A. K.; Feng, S. P. Highly Conductive and Low Cost Ni-PET Flexible Substrate for Efficient Dye-Sensitized Solar Cells. *ACS Appl. Mater. Interfaces* **2014**, *6*, 5577−5584.
(18) Lee, J. Y.; Connor, S. T.; Cui, Y.; Peumans, P. Solution-Processed Metal Nanowire Mesh Transparent Electrodes. *Nano Lett.* **2008**, *8*, 689−692.
(19) De, S.; Higgins, T. M.; Lyons, P. E.; Doherty, E. M.; Nirmalraj, P. N.; Blau, W. J.; Boland, J. J.; Coleman, J. N. Silver Nanowire Networks as Flexible, Transparent, Conducting Films: Extremely High DC to Optical Conductivity Ratios. *ACS Nano* **2009**, *3*, 1767−1774.
(20) Rathmell, A. R.; Bergin, S. M.; Hua, Y. L.; Li, Z. Y.; Wiley, B. J. The Growth Mechanism of Copper Nanowires and Their Properties in Flexible, Transparent Conducting Films. *Adv. Mater.* **2010**, *22*, 3558−3563.
(21) Zou, J.; Yip, H.-L.; Hau, S. K.; Jen, A. K.-Y. Metal Grid/Conducting Polymer Hybrid Transparent Electrode for Inverted Polymer Solar Cells. *Appl. Phys. Lett.* **2010**, *96*, 203301.
(22) Wu, H.; Menon, M.; Gates, E.; Balasubramanian, A.; Bettinger, C. J. Reconfigurable Topography for Rapid Solution Processing of Transparent Conductors. *Adv. Mater.* **2014**, *26*, 706−711.
(23) Hsu, P.-C.; Wang, S.; Wu, H.; Narasimhan, V. K.; Kong, D.; Lee, H. R.; Cui, Y. Performance Enhancement of Metal Nanowire Transparent Conducting Electrodes by Mesoscale Metal Wires. *Nat. Commun.* **2013**, *4*, 2522.
(24) Choi, H. W.; Theodore, N. D.; Alford, T. L. ZnO−Ag−MoO_3 Transparent Composite Electrode for ITO-Free, PEDOT: PSS-Free Bulk-Heterojunction Organic Solar Cells. *Sol. Energy Mater. Sol.Cells* **2013**, *117*, 446−450.
(25) Xu, W.-F.; Chin, C.-C.; Hung, D.-W.; Wei, P.-K. Transparent Electrode for Organic Solar Cells Using Multilayer Structures with Nanoporous Silver Film. *Sol. Energy Mater. Sol. Cells* **2013**, *118*, 81−89.
(26) Guo, X.; Lin, J.; Chen, H.; Zhang, X.; Fan, Y.; Luo, J.; Liu, X. Ultrathin and Efficient Flexible Polymer Photovoltaic Cells Based on Stable Indium-Free Multilayer Transparent Electrodes. *J. Mater. Chem.* **2012**, *22*, 17176−17182.
(27) Yun, J.; Wang, W.; Bae, T. S.; Park, Y. H.; Kang, Y. C.; Kim, D. H.; Lee, S.; Lee, G. H.; Song, M.; Kang, J. W. Preparation of Flexible Organic Solar Cells with Highly Conductive and Transparent Metal-Oxide Multilayer Electrodes Based on Silver Oxide. *ACS Appl. Mater. Interfaces* **2013**, *5*, 9933−9941.
(28) Park, Y.-S.; Park, H.-K.; Kim, J.-Z.; Choi, K.-H.; Na, S.-I.; Kim, D.-Y. Comparative Investigation of Transparent ITO/Ag/ITO and ITO/Cu/ITO Electrodes Grown by Dual-Target DC Sputtering for Organic Photovoltaics. *J. Electrochem. Soc.* **2009**, *156*, H588−H594.
(29) Choi, Y.-Y.; Choi, K.-H.; Lee, H.; Lee, H.; Kang, J.-W.; Kim, H.-K. Nano-Sized Ag-Inserted Amorphous $ZnSnO_3$ Multilayer Electrodes for Cost-Efficient Inverted Organic Solar Cells. *Sol. Energy Mater. Sol. Cells* **2011**, *95*, 1615−1623.
(30) Winkler, T.; Schmidt, H.; Flügge, H.; Nikolayzik, F.; Baumann, I.; Schmale, S.; Weimann, T.; Hinze, P.; Johannes, H.-H.; Rabe, T.; Hamwi, S.; Riedl, T.; Kowalsky, W. Efficient Large Area Semi-transparent Organic Solar Cells Based on Highly Transparent and Conductive ZTO/Ag/ZTO Multilayer Top Electrodes. *Org. Electron.* **2011**, *12*, 1612−1618.
(31) Ryu, S. Y.; Noh, J. H.; Hwang, B. H.; Kim, C. S.; Jo, S. J.; Kim, J. T.; Hwang, H. S.; Baik, H. K.; Jeong, H. S.; Lee, C. H.; Song, S. Y.; Choi, S. H.; Park, S. Y. Transparent Organic Light-Emitting Diodes Consisting of a Metal Oxide Multilayer Cathode. *Appl. Phys. Lett.* **2008**, *92*, 023306.
(32) Schubert, S.; Meiss, J.; Müller-Meskamp, L.; Leo, K. Improvement of Transparent Metal Top Electrodes for Organic Solar Cells by Introducing a High Surface Energy Seed Layer. *Adv. Energy Mater.* **2013**, *3*, 438−443.
(33) Sergeant, N. P.; Hadipour, A.; Niesen, B.; Cheyns, D.; Heremans, P.; Peumans, P.; Rand, B. P. Design of Transparent Anodes for Resonant Cavity Enhanced Light Harvesting in Organic Solar Cells. *Adv. Mater.* **2012**, *24*, 728−732.
(34) Yoo, B.; Kim, K.; Lee, S. H.; Kim, W. M.; Park, N.-G. ITO/ATO/TiO_2 Triple-Layered Transparent Conducting Substrates for Dye-Sensitized Solar Cells. *Sol. Energy Mater. Sol. Cells* **2008**, *92*, 873−877.
(35) Wang, W.; Song, M.; Bae, T.-S.; Park, Y. H.; Kang, Y.-C.; Lee, S.-G.; Kim, S.-Y.; Kim, D. H.; Lee, S.; Min, G.; Lee, G.-H.; Kang, J.-W.; Yun, J. Transparent Ultrathin Oxygen-Doped Silver Electrodes for Flexible Organic Solar Cells. *Adv. Funct. Mater.* **2014**, *24*, 1551−1561.
(36) Zhai, Z.; Huang, X.; Xu, M.; Yuan, J.; Peng, J.; Ma, W. Greatly Reduced Processing Temperature for a Solution-Processed NiO_x

Buffer Layer in Polymer Solar Cells. *Adv. Energy Mater.* **2013**, *3*, 1614−1622.
(37) Bai, S.; Cao, M.; Jin, Y.; Dai, X.; Liang, X.; Ye, Z.; Li, M.; Cheng, J.; Xiao, X.; Wu, Z.; Xia, Z.; Sun, B.; Wang, E.; Mo, Y.; Gao, F.; Zhang, F. Low-Temperature Combustion-Synthesized Nickel Oxide Thin Films as Hole-Transport Interlayers for Solution-Processed Optoelectronic Devices. *Adv. Energy Mater.* **2014**, *4*, 10.1002/aenm.201301460.
(38) Cattin, L.; Bernède, J. C.; Morsli, M. Toward Indium-Free Optoelectronic Devices: Dielectric/Metal/Dielectric Alternative Transparent Conductive Electrode in Organic Photovoltaic Cells. *Phys. Status Solidi A* **2013**, *210*, 1047−1061.
(39) Ellmer, K. Past Achievements and Future Challenges in the Development of Optically Transparent Electrodes. *Nat. Photonics* **2012**, *6*, 809−817.
(40) Bernède, J. C.; Cattin, L.; Morsli, M.; Berredjem, Y. Ultra-Thin Metal Layer Passivation of the Transparent Conductive Anode in Organic Solar Cells. *Sol. Energy Mater. Sol. Cells* **2008**, *92*, 1508−1515.
(41) Wang, N.; Liu, X.; Liu, X. Ultraviolet Luminescent, High-Effective-Work-Function $LaTiO_3$-Doped Indium Oxide and Its Effects in Organic Optoelectronics. *Adv. Mater.* **2010**, *22*, 2211−2215.
(42) Schubert, S.; Meiss, J.; Meskamp, L. M.; Leo, K. Improvement of Transparent Metal Top Electrodes for Organic Solar Cells by Introducing a High Surface Energy Seed Layer. *Adv. Energy Mater.* **2013**, *3*, 438−443.
(43) Ratcliff, E. L.; Meyer, J.; Steirer, K. X.; Garcia, A.; Berry, J. J.; Ginley, D. S.; Olson, D. C.; Kahn, A.; Armstrong, N. R. Evidence for Near-Surface NiOOH Species in Solution-Processed NiO_x Selective Interlayer Materials: Impact on Energetics and the Performance of Polymer Bulk Heterojunction Photovoltaics. *Chem. Mater.* **2011**, *23*, 4988−5000.